Materials Advances

ROYAL SOCIETY OF CHEMISTRY

PAPER

View Article Online
View Journal | View Issue

Cite this: *Mater. Adv.*, 2025, 6, 2002

Unzipped MWCNT/polypyrrole hybrid composites: a pathway to high-performance asymmetric supercapacitors†

Shilpa Simon, Letcy V. Theresa and Sreeja P. B. *

A novel method has been developed for the conversion of multi-walled carbon nanotubes (MWCNTs) into unzipped MWCNTs (UzMWCNT) using a modified Hummer's method followed by reduction. This technique allows for the controlled modification of MWCNTs in both transverse and longitudinal directions. The UzMWCNT exhibits unique structural characteristics that combine the properties of 1D nanotubes and graphene-like features. The UzMWCNT/PPy composite exhibited an impressive specific capacitance of 944 F g^{-1} along with excellent cycling stability, retaining 92% of its capacitance after 5000 cycles. For the UzMWCNT/PPy//AC composite, the gravimetric capacitance decreased with increasing current density, from 400 F g^{-1} at 1.0 A g^{-1} to 162 F g^{-1} at 2.5 A g^{-1}. Furthermore, the UzMWCNT/PPy//AC composite demonstrated outstanding long-term durability, retaining approximately 95% of its capacitance after 5000 cycles at a current density of 5 A g^{-1}, underscoring its excellent cycling stability. This research paves the way for the development of high-performance supercapacitor electrodes using hybrid materials derived from MWCNTs.

Received 20th December 2024,
Accepted 19th February 2025

DOI: 10.1039/d4ma01270d

rsc.li/materials-advances

1. Introduction

To meet the demands of sustainable societal development, researchers are continuously exploring advancements in renewable energy.[1–3] Batteries and supercapacitors represent two of the most promising directions and are widely utilized as energy storage devices.[4–6] Electrochemical capacitors, or supercapacitors, offer significant advantages over traditional batteries, including longer life cycles, rapid power delivery and absorption, high power density, and excellent energy reversibility.[7–11] Due to these features, supercapacitors are becoming a preferred energy storage solution for various applications, such as hybrid electric vehicles, portable electronics, and energy management systems.[12–14] However, their overall performance is largely determined by the choice of electrode materials, which directly affects the device's capacity, power delivery, and durability.[15–17] Carbon-based materials, in particular, are essential for meeting the growing demand for efficient energy storage solutions.[18–21]

In this context, carbon nanotubes (CNTs) have emerged as promising candidates for supercapacitor electrodes owing to their well-defined nanostructure, high electrical conductivity, and chemical stability.[22–26] However, conventional CNTs are typical of micrometre-scale lengths and tend to aggregate into tangled bundles, impeding ion transport within the tubes, especially in the case of MWCNTs.[27] Consequently, this limits any significant improvement in the specific capacitance of supercapacitors. To fully harness the exceptional properties of CNTs, methods for macroscopic modification are required.[28–30] MWCNTs exhibit excellent intrinsic conductivity; however, their tubular structure often leads to agglomeration and limited surface accessibility, which can hinder their electrochemical performance.[31–33]

Recent advances in CNT manipulation have led to the production of shorter fragments and nanoribbons through cutting processes.[34] Various techniques have been employed to shorten long CNTs, including ball milling, cryogenic crushing, solid-state reactions, selective etching, fluorination, chemical oxidation, and electrochemical methods.[35–37] Short segments obtained from transverse cutting have demonstrated superior performance in energy applications.[38] Additionally, longitudinal unzipping of CNTs has been achieved through processes like plasma etching, oxidative treatment, electrochemical approaches, potassium vapour treatment, and catalytic hydrogenation.[39–43] Despite these advancements, the one-step cutting and unzipping of CNTs in both directions remains challenging due to complex procedures and intricate manipulation.[38] However, the potential for improved electrochemical reactivity with open-ended CNTs has been observed. Thus, there is a persistent need to develop effective strategies for simultaneously cutting and splitting CNTs.[44]

Department of Chemistry, Christ University, Bengaluru 560029, India.
E-mail: sreeja.pb@christuniversity.in

† Electronic supplementary information (ESI) available. See DOI: https://doi.org/10.1039/d4ma01270d

We utilized a cost-efficient, modified Hummer's method to process MWCNTs.[45,46] Our results indicate that the MWCNTs were cut transversely and unzipped longitudinally, leading to the formation of curved graphene nanostructures, which may exhibit a structure partially resembling interconnected graphene fragments.

Conductive polymer–CNT exhibits remarkable electrochemical performance when used as supercapacitor electrodes.[47] Among the most promising conductive polymers, researchers have shown particular interest in polyaniline (PANI),[48] polypyrrole (PPy),[49] polythiophene (PTh),[50] and their modified versions. PPy is notable for its high conductivity, excellent redox reversibility, and eco-friendliness.[51–53] However, it is plagued by issues of swelling and degradation of polymer chains, which result in inadequate cycling stability.[54,55]

To address these limitations, UzMWCNT has been incorporated into the PPy matrix to enhance the mechanical, thermal, and electrical conductivity of the composites. This improvement arises from the synergistic interactions between the constituent elements. UzMWCNT boasts both superior electrical conductivity and mechanical strength, while also promoting efficient charge transport. This translates to speedy charging and discharging capabilities in supercapacitors.[56] Various methods are used for preparing composites of CNTs and conductive polymers such as electrochemical methods,[57] microemulsion polymerization,[58] vapor-phase polymerization,[59] and *in situ* polymerization.[60] *In-situ* polymerization plays a crucial role in the production of conducting polymers and carbon-based materials for supercapacitors.[53–55] This innovative technique allows for the controlled synthesis of polymers and carbon structures directly within the desired application, resulting in enhanced performance and tailored properties.[61,62]

In this study, we employ a modified Hummer's method to achieve the cutting and unzipping of CNTs, utilizing cost-effective MWCNTs as raw materials resulting in the formation of UzMWCNT. This report outlines a one-step synthesis method for preparing UzMWCNT/PPy composites. The process involves interfacial polymerization of pyrrole conducted within solvents containing UzMWCNT. The primary benefit of utilizing interfacial polymerization for the synthesis of nanocomposite materials, in general, lies in the exceptionally slow reaction rate. This characteristic allows for precise encapsulation of nanostructures like UzMWCNT in this instance, resulting in improved dispersion within the polymer matrix, making it highly promising for supercapacitor applications.

2. Materials and methods

2.1. Materials

Multi-walled carbon nanotubes (MWCNTs >95.0%), pyrrole (monomer 99.5%), ammonium persulfate (APS, ≥98%), sodium nitrate ($NaNO_3$), sulfuric acid (H_2SO_4), potassium permanganate ($KMnO_4$), hydrogen peroxide (H_2O_2), sodium borohydride ($NaBH_4$), and hydrochloric acid (HCl) were purchased from Sigma-Aldrich. All chemicals were high-grade reagents and were used as received.

2.2. UzMWCNT/PPy

The synthesis of UzMWCNT/PPy was carried out using a two-step process consisting of hydrothermal treatment and surface functionalization, ensuring a straightforward and cost-effective methodology.

2.2.1. Synthesis of UzMWCNT. The fabrication of UzMWCNTs involves a sequential two-step process consisting of oxidation and reduction stages. Initially, MWCNTs undergo oxidation using a modified Hummer's method. This initial stage begins by dispersing 4 g of MWCNTs and 2 g of $NaNO_3$ in a 500 mL flask containing concentrated H_2SO_4 (98%). The mixture is then stirred in an ice bath for 1 hour to maintain a controlled temperature environment. Subsequently, 1 M $KMnO_4$ solution is gradually added to the suspension, ensuring the reaction temperature remains below 20 °C. After removing the ice bath, the mixture is stirred at room temperature for an additional hour to facilitate the oxidation process. Next, deionized (DI) water is slowly added under vigorous stirring, followed by a 30-minute stirring period of the diluted suspension. The final step of the oxidation stage involves the addition of 20 mL of 30% H_2O_2 and 280 mL of DI water. The resulting mixture undergoes multiple cycles of washing and centrifugation with 10% HCl and deionized water until a neutral pH is achieved. Finally, vacuum drying yields oxidized MWCNTs (O-MWCNTs) as a black powder, with a typical yield of approximately 80% based on the starting CNTs. This oxidized material then serves as the precursor for the subsequent reduction step, ultimately leading to the formation of the desired UzMWCNTs.[38]

Next, the O-MWCNTs (100 mg) were dispersed in 100 mL of water through ultrasonic treatment for 1 hour. Subsequently, 500 mg of $NaBH_4$ was gradually added to the mixture, which was then stirred for 24 hours at room temperature. The solid sample was collected after washing with ethanol and DI water and subjected to vacuum drying at 60 °C, resulting in the formation of the UzMWCNT material.[63]

2.2.2. Synthesis of UzMWCNT/polypyrrole. The UzMWCNT (5 wt%) suspension underwent ultrasonication for 30 minutes. Following sonication, 1 mL of PPy dispersion was introduced drop by drop into the suspensions and stirred for 30 minutes at a speed of 500 rpm. Subsequently, APS was incorporated into the mixture, and continuous stirring was maintained for another 30 minutes. To allow the polymerization reaction to progress, the mixture was stirred for 24 hours at a temperature of 0 °C. After this period, black powders were collected and subjected to multiple washes with DI water and ethanol to eliminate impurities. The final products were then vacuum-dried at 60 °C for 24 hours.[64]

2.3. Characterization methods

The structural and morphological properties of UzMWCNT and UzMWCNT/PPy composites were comprehensively analyzed using advanced analytical techniques. The microstructure and surface morphology of the samples were investigated using scanning electron microscopy (SEM) (Nova Nano SEM 450) and high-resolution transmission electron microscopy (HRTEM)

(JEM-2100). X-ray diffraction (XRD) analysis was conducted using a Rigaku XRD diffractometer, covering a wide angular range (5–80°) to identify the crystalline phases and assess the structural modifications induced by the composite formation. Raman spectroscopy, performed using a 532 nm Renishaw Raman system, further confirmed the structural characteristics, providing information on the graphitic structure and disorder in the materials. To determine the elemental composition and chemical bonding states, X-ray photoelectron spectroscopy (XPS) was carried out using a K-Alpha spectrometer (KAN9954133). The specific surface area, pore volume, and pore size distribution of the samples were determined using the Brunauer–Emmett–Teller (BET) method, conducted with a BELSORP MINI X analyser.

2.4. Supercapacitor electrode preparation and testing

The preparation of supercapacitor electrodes involved coating electrode-active materials onto a nickel foam substrate using the doctor blade method. The electrode composition consisted of an electrode-active material (85 wt%), polyvinylidene fluoride (PVDF, 10 wt%), and carbon black (5 wt%). To prepare a uniform slurry, the electrode-active material, PVDF, and carbon black were mixed with *N*-methyl pyrrolidine (NMP) solvent using a lab-scale mortar and pestle. This slurry was then evenly coated onto nickel foam and dried overnight in a vacuum oven at 80 °C to ensure complete solvent removal. The electrochemical performance was evaluated in a three-electrode cell configuration. The electrode-active material-coated nickel foam served as the working electrode, with platinum wire as the counter electrode and Ag/AgCl (saturated KCl) as the reference electrode. All electrochemical tests were performed using an electrochemical workstation potentiostat (CHI608E). Electrochemical evaluations included cyclic voltammetry (CV), galvanostatic charge–discharge (GCD), and electrochemical impedance spectroscopy (EIS).

2.5. Asymmetric supercapacitor fabrication and testing

An asymmetric supercapacitor was fabricated to evaluate the potential application of the UzMWCNT/PPy//AC nanocomposite in energy storage devices. The device was assembled with a UzMWCNT/PPy-based positive electrode and an active carbon (AC)-based negative electrode. Aqueous 3 M KOH was used as the electrolyte, ensuring efficient ion conductivity and stability during testing. The as-fabricated UzMWCNT/PPy//AC asymmetric supercapacitor cell underwent electrochemical testing using EIS, CV, and GCD techniques.

3. Results and discussion

3.1. Structure of the UzMWCNT/PPy nanocomposite

The functionalization of UzMWCNT through PPy and interfacial polymerization was analyzed using XRD, as shown in Fig. 1a. The XRD patterns highlight the structural changes occurring in pristine MWCNTs, UzMWCNTs, and UzMWCNT/PPy composites. In pristine MWCNTs, sharp diffraction peaks corresponding to the (002) and (100) planes indicate a well-ordered graphitic structure with a *d*-spacing of 0.34 nm. Upon unzipping and functionalization, the UzMWCNT sample exhibited a broader (002) peak at 26.2°, corresponding to an increased interlayer spacing of approximately 0.37 nm, likely due to the introduction of oxygen-containing functional groups and structural defects. Additionally, a broad peak at 43.3° attributed to the (100) plane suggests turbostratic disorder within the UzMWCNT framework.

The XRD spectrum of UzMWCNT/PPy demonstrates significant modifications, including a broad peak in the range of 20°–30°, centered at 26.4°, which is characteristic of pyrrole monomers. This peak appears sharper compared to pure PPy, indicating potential synergistic electronic interactions between PPy chains and the UzMWCNT substrate. The merging of diffraction peaks from UzMWCNT and PPy in the composite reflects its predominantly amorphous nature, which is favorable for supercapacitor applications. The amorphous structure enhances the interaction between the polymerized PPy and UzMWCNT, allowing for increased electrolyte ion accessibility and facilitating redox reactions. The observed reduction in crystallinity upon PPy functionalization suggests an improved electrochemical activity. This enhancement is attributed to the polymerization of PPy on the high-surface-area UzMWCNT nanosheets, enabling better ion diffusion and redox reaction kinetics.

Raman spectroscopy was utilized to analyze the chemical bonding and structural characteristics of the UzMWCNT and UzMWCNT/PPy composites, as shown in Fig. 1b. The spectra reveal the characteristic D band at 1349 cm^{-1}, indicative of

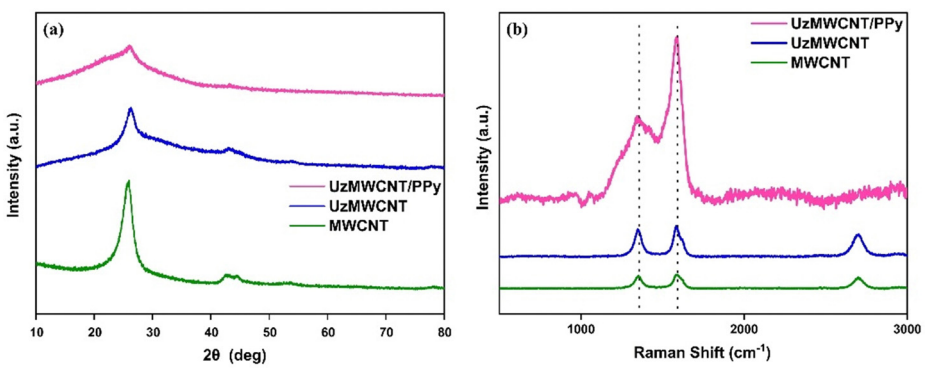

Fig. 1 (a) XRD and (b) Raman spectra of MWCNTs, UzMWCNTs, and the UzMWCNT/PPy nanocomposites.

structural defects, and the G band at 1584 cm^{-1}, corresponding to the in-plane stretching vibrations of sp^2-hybridized carbon atoms in both ring and chain configurations. The presence of these peaks confirms the graphitic structure of the carbon materials. For the UzMWCNT/PPy composite, a noticeable decrease in the intensity of the G band (sp^2 domains) was observed, suggesting significant modifications to the carbon structure due to functionalization with PPy. The intensity ratio (I_D/I_G) of the D peak to the G peak in UzMWCNT/PPy is higher compared to that for pristine UzMWCNT, indicating the introduction of abundant structural defects during the carbonization and activation processes. These structural defects enhance the surface reactivity and facilitate the interaction between UzMWCNT and PPy. The Raman spectra also confirm the successful growth of PPy onto the UzMWCNT substrate, as evidenced by the retention of characteristic signals from both components. This result aligns well with the findings from XRD analysis, corroborating the structural and compositional changes induced by the polymerization of PPy on the UzMWCNT framework. The synergistic combination of PPy and UzMWCNT enhances the composite's structural and electrochemical properties, making it a promising candidate for energy storage applications.

XPS was performed to analyze the elemental composition and chemical bonding states in the UzMWCNT/PPy composite, as shown in Fig. (2a–d). The survey spectrum (Fig. 2a) reveals prominent peaks corresponding to C 1s, N 1s, and O 1s, confirming the presence of carbon, nitrogen, and oxygen elements within the composite. These elements are indicative of both the UzMWCNT and the PPy functional groups.

The high-resolution C 1s spectrum was deconvoluted into four main peaks (Fig. 2b). The peak at 284.49 eV corresponds to C–C bonds, indicative of the graphitic carbon backbone. The peak at 283.94 eV represents C═C bonds, confirming the sp^2-hybridized carbon framework. Peaks at 285.09 eV and 286.34 eV are assigned to C–N/C–O and C═N/C═O bonds, respectively, highlighting the presence of oxygen and nitrogen functional groups. These peaks confirm the successful functionalization of UzMWCNT with PPy. The O 1s spectrum shows two distinct peaks at 531.49 eV and 532.49 eV, corresponding to C═O and C–O bonds,[65] respectively (Fig. 2c). These oxygen-containing groups are likely introduced during the oxidation and functionalization processes, contributing to enhanced surface reactivity and improved electrochemical properties of the composite. The N 1s spectrum was deconvoluted into two main peaks at 399.59 eV and 400.09 eV, corresponding to C═N and C–NH bonds,[66] respectively (Fig. 2d). These nitrogen-containing bonds originate from the PPy polymer and indicate successful integration of PPy with UzMWCNT. The presence of nitrogen also enhances the pseudocapacitive behavior of the composite.

The XPS analysis confirms the successful incorporation of functional groups from both UzMWCNT and PPy, indicating the formation of a stable composite. The nitrogen and oxygen functionalities play a critical role in enhancing the

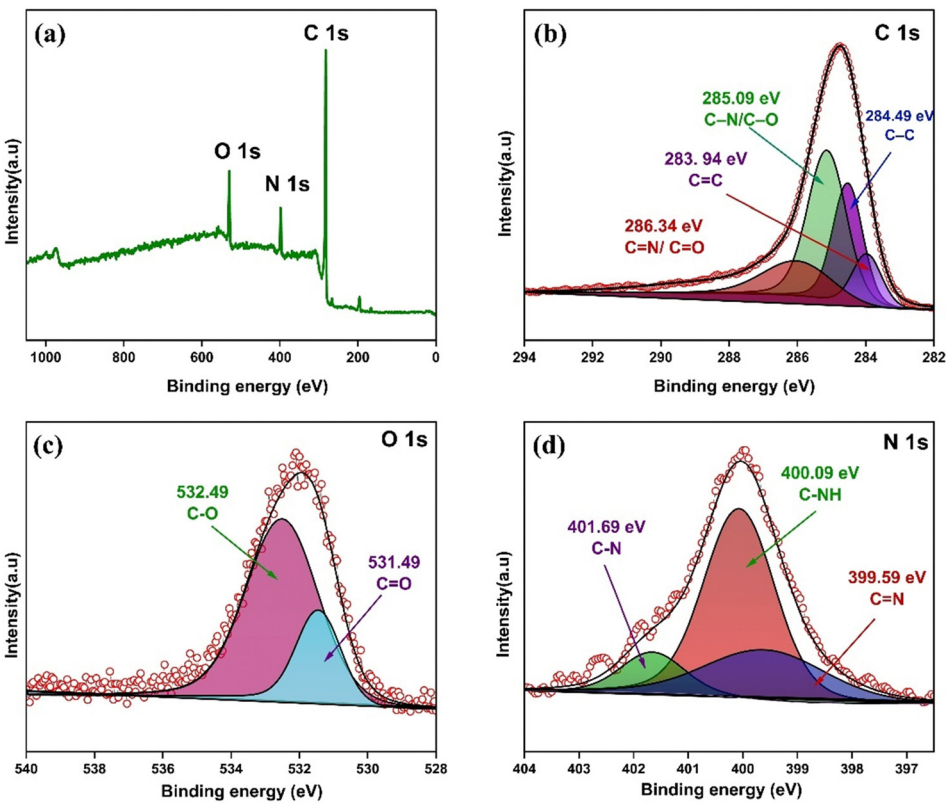

Fig. 2 Deconvoluted XPS spectra of UzMWCNT/PPy: (a) survey spectra, (b) C 1s, (c) O 1s, and (d) N 1s.

electrochemical performance by increasing active sites for redox reactions and improving wettability for better interaction with electrolytes. Combining carbon materials with pseudocapacitive materials such as conducting polymers and organic moieties could help to achieve enhanced capacitance and improved rate capabilities.

The surface area and pore characteristics of the synthesized nanomaterials were analyzed using N_2 adsorption–desorption isotherms and BJH pore size distribution, as shown in Fig. 3. The study revealed significant changes in textural properties resulting from unzipping and functionalization processes, particularly with the introduction of PPy.

All the materials exhibited type IV isotherms with distinct hysteresis loops at higher relative pressures, indicative of mesoporous structures. For pristine MWCNT, the BET surface area was determined to be 90 $m^2\ g^{-1}$, reflecting its baseline porosity and surface characteristics (Fig. 3a). After unzipping, UzMWCNT displayed enhanced adsorption, with a BET surface area of 120 $m^2\ g^{-1}$, attributed to structural modifications and defect generation (Fig. 3b). Further functionalization with PPy resulted in an increase in surface area to 168 $m^2\ g^{-1}$ for UzMWCNT/PPy, highlighting the significant impact of PPy incorporation in creating additional active sites and improving pore accessibility (Fig. 3c).

The BJH analysis (Fig. 3d–f) confirmed the presence of mesoporous structures, with pore sizes predominantly in the range of 2–50 nm for all samples. The cumulative pore volume and distribution broadened for UzMWCNT (BET surface area 120 $m^2\ g^{-1}$) compared to pristine MWCNT, indicating the introduction of additional porosity during the unzipping process. The UzMWCNT/PPy composite showed the highest cumulative pore volume and a well-defined mesoporous network, correlating with its BET surface area of 168 $m^2\ g^{-1}$. The presence of large mesopores improves ionic transport, enabling the efficient formation of an electrical double layer, while the functionalization with PPy further expands the pore structure and creates interconnected networks, enhancing ion transport and electrolyte diffusion, thereby improving the interaction between faradaic materials and the electrolyte.

3.2. Microstructure and surface morphology of the UzMWCNT/PPy nanocomposite

The microstructure and surface morphology of the synthesized UzMWCNT and UzMWCNT/PPy composites were analyzed using SEM, as shown in Fig. 4(a–d).

Fig. 4(a) and (b) depict the SEM images of UzMWCNT, which reveal an intricate, entangled network of nanotubes with visible bundling and a porous morphology. The fine, tubular, and interconnected structure observed highlights the nanoscale features of the UzMWCNT. This morphology is particularly beneficial as it provides a high surface area, facilitating enhanced electron and ion transport – key attributes for supercapacitor electrode performance.

In Fig. 4(c) and (d), the SEM images of the UzMWCNT/PPy composite show the successful integration of PPy into the UzMWCNT framework. The porous and interconnected network structure is preserved, while the presence of PPy is clearly visible, as indicated in Fig. 4d. The uniform coating of PPy enhances the overall conductivity and introduces pseudocapacitive behavior to the composite, leading to a synergistic effect. This combination of UzMWCNT's high conductivity and PPy's redox-active properties significantly improves the energy storage capacity of the material.

The TEM images provide detailed insights into the microstructure and polymerization behavior of PPy over UzMWCNT. As observed in Fig. 5a, the UzMWCNT framework displays a well-defined tubular morphology with dimensions of approximately 35.19 nm, confirming its nanoscale structure. The uniform

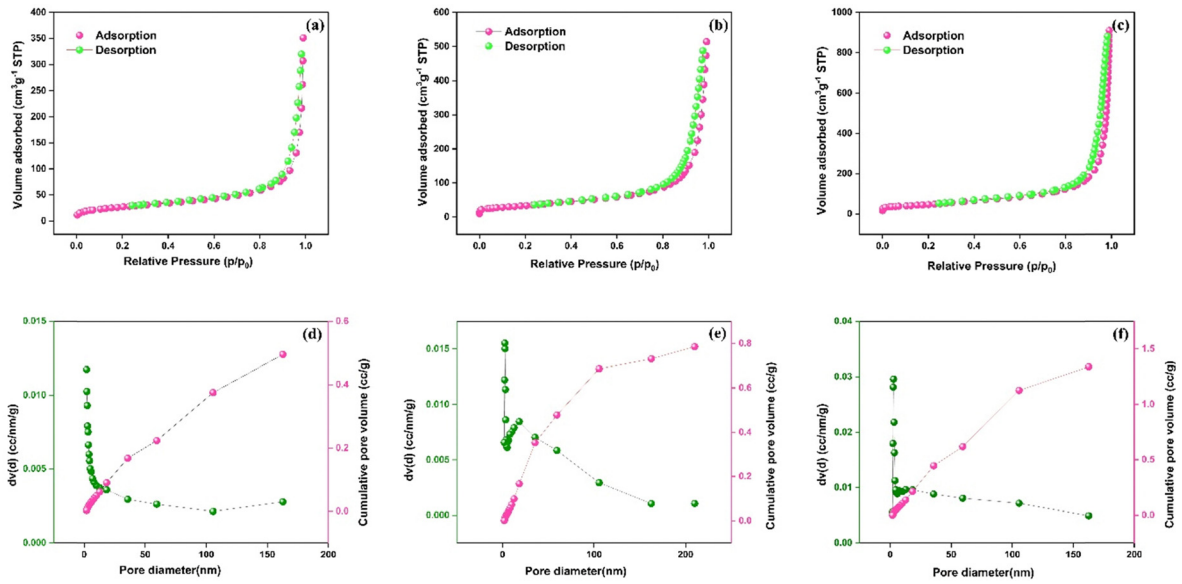

Fig. 3 N_2 adsorption–desorption isotherm: (a) MWCNT; (b) UzMWCNT; and (c) UzMWCNT/PPy; and BJH plot of (d) MWCNT; (e) UzMWCNT; and (f) UzMWCNT/PPy.

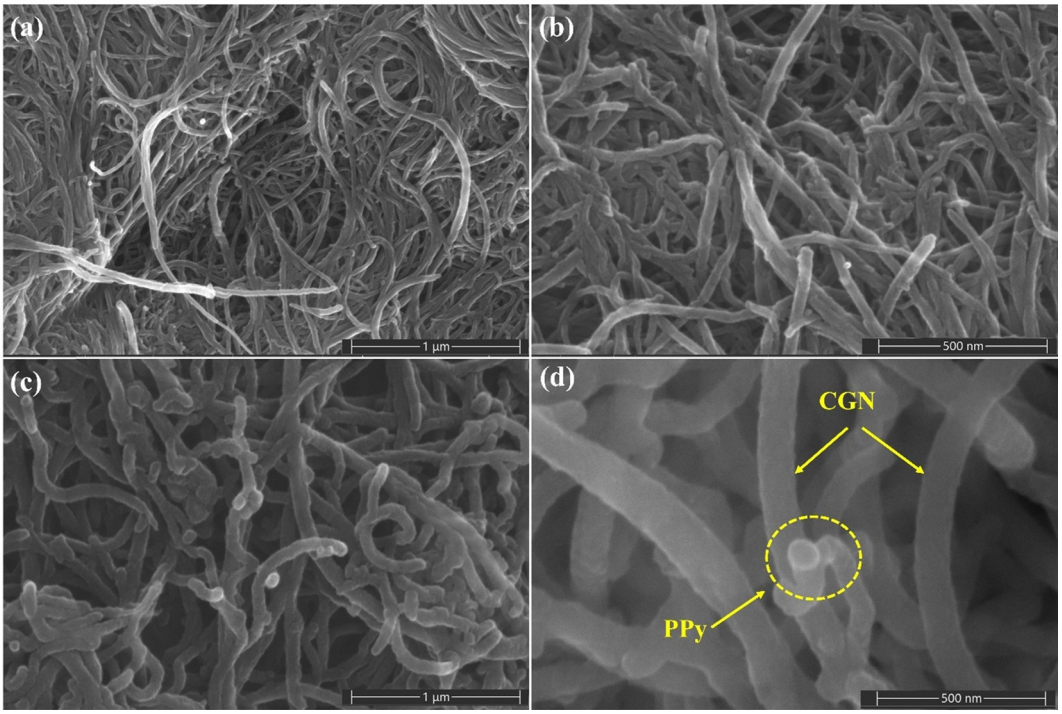

Fig. 4 SEM image of (a and b) UzMWCNT and (c and d) UzMWCNT/PPy.

polymerization of PPy onto the UzMWCNT surface is evident, highlighting the successful formation of the UzMWCNT/PPy composite. The selected area electron diffraction (SAED) pattern (Fig. 5c) exhibits characteristic diffraction rings, confirming the amorphous nature of the composite. In the high-resolution TEM image (Fig. 5d), the interlayer spacing of 0.37 nm is distinctly visible, indicating the presence of structural modifications, which can be attributed to the unzipping and subsequent functionalization of MWCNTs. This suggests the formation of well-integrated UzMWCNT/PPy, where the synergistic combination of the tubular carbon framework and polymerized PPy enhances conductivity and redox activity. These structural changes facilitate improved surface area and active sites for ion interaction, which are essential for enhanced electrochemical performance in energy storage applications.

3.3. Electrochemical evaluation of UzMWCNT/PPy composite electrodes

To further assess the electrochemical performance of both UzMWCNT and UzMWCNT/PPy, we conducted CV experiments and the results are shown in Fig. 6. In Fig. 6a, the enclosed area under the CV curves is larger for UzMWCNT/PPy compared to UzMWCNT at 5 mV s^{-1}. In contrast, curves clearly exhibit redox peaks, indicating that the UzMWCNT/PPy composite demonstrates pseudocapacitive behaviour. Response current rises continuously with increasing scan rates, suggesting that ionic and electronic transport rates are fast enough at these scan rates. This emphasizes the remarkable kinetics and reversibility of the UzMWCNT/PPy combination. This indicates that the UzMWCNT/PPy composite exhibits a higher charge storage capability, attributed to the synergistic effect between the conducting PPy matrix and the UzMWCNT. The presence of well-defined redox peaks in the UzMWCNT/PPy curves confirms the occurrence of pseudocapacitive behavior, highlighting the contribution of faradaic reactions in addition to the EDLC of UzMWCNT. The enhanced redox activity can be associated with the reversible doping/dedoping processes of PPy, which further contributes to charge storage capacity.

The CV curves in Fig. 6b were generated by varying the scan rates from 5 to 100 mV s^{-1} within a potential range of −0.4 to 0.6 V. Additionally, as the scan rate increases, the shape of these CV curves remains consistent, suggesting that the UzMWCNT/PPy composites possess good ionic and electronic conductivity.

Fig. 6c illustrates the galvanostatic charge/discharge curves for both the UzMWCNT and UzMWCNT/PPy composites. The fact that the UzMWCNT/PPy composite exhibits the longest discharge time indicates that it exhibits the highest electrochemical performance. In Fig. 6b, the galvanostatic charge/discharge curves for UzMWCNT/PPy are depicted at varying current densities. The specific capacitances at different current densities were determined using eqn (1).[67] These curves exhibit a nearly linear behavior, suggesting that the composite displays good symmetry and minimal internal resistance (iR drops), supporting the notion that the unzipping process enhances electron mobility and facilitates faster charge propagation which are characteristics associated with a high-quality capacitor.[68]

$$C_{sp} = \frac{I \times \Delta t}{m \times \Delta v} \quad (1)$$

The UzMWCNT/PPy electrode exhibits a specific capacitance of 944 F g^{-1} at a current density of 1 A g^{-1}. This high specific

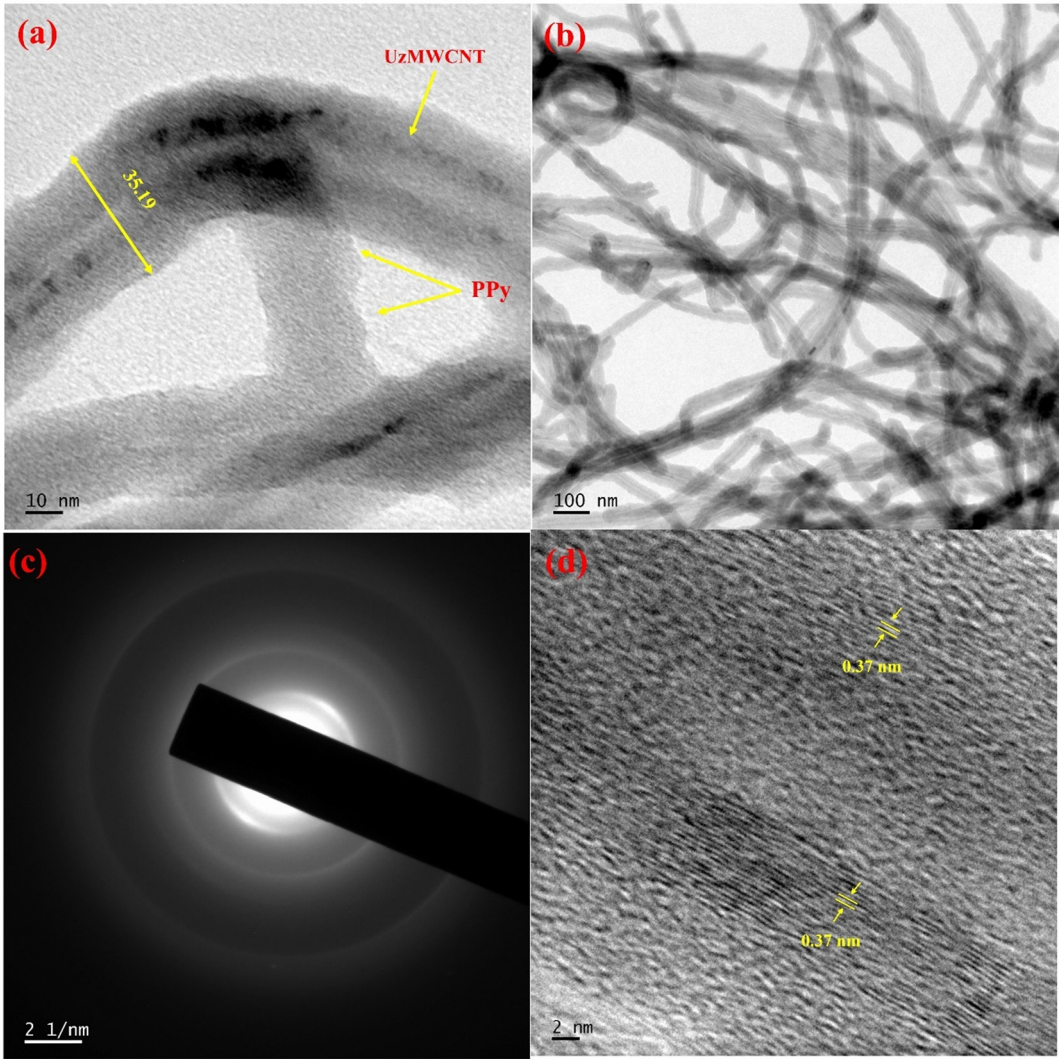

Fig. 5 TEM analysis of the UzMWCNT/PPy nanocomposite; (a) and (b) nanocomposite at two different magnifications; (c) SAED pattern; and (d) HR-TEM image.

capacitance arises from the synergistic interaction between UzMWCNT and PPy in the nanocomposite. The large surface area of UzMWCNT nanosheets supports uniform polymerization of PPy, enhancing pseudocapacitive charge storage. A decline in specific capacitance is observed with increasing current density, which can be attributed to the limited reaction kinetics of the electrode at higher current densities. To evaluate the contribution of PPy in the composite, the specific capacitance of UzMWCNT/PPy was measured at different current densities of 1, 2, 3, and 4 A g^{-1}, yielding values of 944, 350, 205, and 157 F g^{-1}, respectively (Fig. 6d). A comparison of various modified MWCNT based nanocomposite electrodes is given in Table 1.

Additionally, the non-linear curves, which match the observed redox peaks in the CV curves, provide additional evidence for the composite's pseudocapacitive nature. This suggests that UzMWCNT/PPy exhibits good charge and discharge reversibility when used as an electrode material for a supercapacitor. At the interface between the electrolyte and the active material of the electrode, electric charge can be efficiently stored and released.

In order to verify UzMWCNT/PPy's exceptional electrochemical capabilities, impedance is performed (Fig. 7a). The circular arc radius of UzMWCNT/PPy composites is clearly smaller in the high-frequency range than that of pure UzMWCNT, suggesting a reduced internal resistance in the UzMWCNT/PPy composites. UzMWCNT/PPy composites show a steeper slope in the low-frequency region than PPy, which suggests quicker ion exchange during charge and discharge. The UzMWCNT's tubular hollow structure and network arrangement, which provide more electrolyte ion freedom throughout the exchange process, are responsible for this improved ion exchange. These results confirm that the electrochemical performance of supercapacitors is greatly improved by UzMWCNT/PPy composites. The increased resistance observed in UzMWCNT/PPy is primarily due to PPy's relatively poor electrical conductivity in a KOH electrolyte. However, the UzMWCNT/PPy composite demonstrates excellent rate capability. In the low-frequency region (below 1 Hz), the linear portion of the impedance curve corresponds to Warburg diffusion impedance (ZW) within the electrolyte, indicating capacitor-like behaviour. A longer ZW line suggests restricted

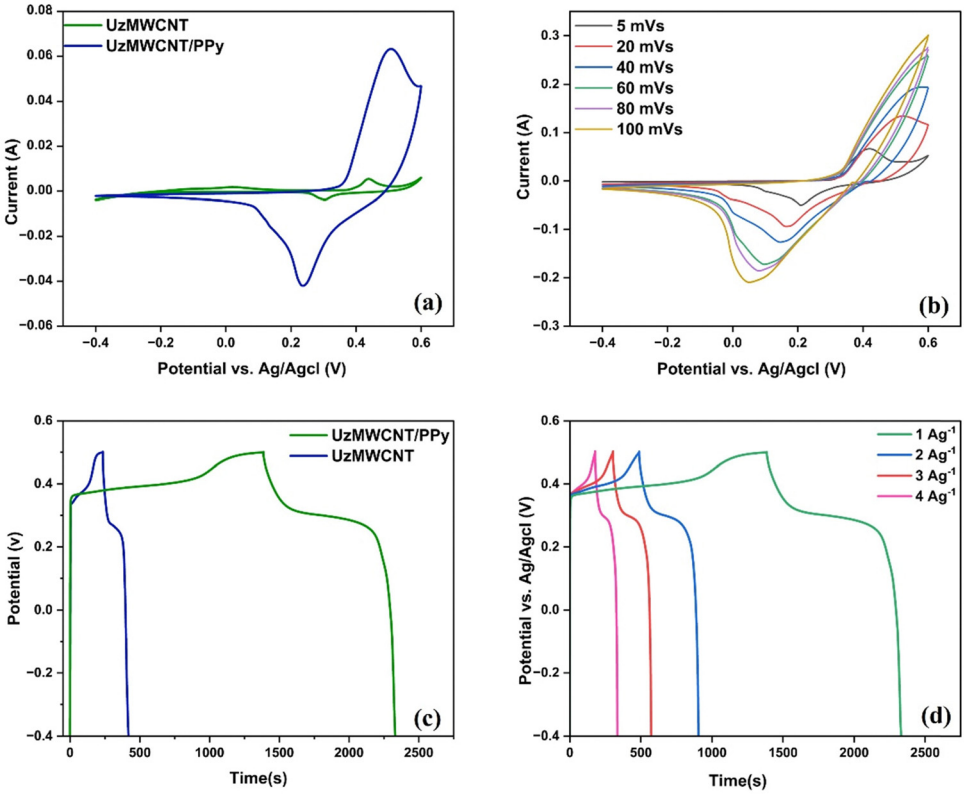

Fig. 6 (a) Cyclic voltammograms of UzMWCNT and UzMWCNT/PPy nanocomposites at a fixed scan rate of 50 mV s^{-1}; (b) CV curves of the UzMWCNT/PPy nanocomposite electrode at varying scan rates; (c) GCD profiles of UzMWCNT and UzMWCNT/PPy nanocomposites; and (d) GCD curves of UzMWCNT/PPy nanocomposite electrodes at different current densities.

Table 1 A comparison of various modified MWCNT based nanocomposite electrodes

Electrode material	Synthesis method	Gravimetric capacitance (F g^{-1})	Cycling stability (cycles)	Ref.
Graphene/CNT-PANI electrode	Electrodeposition	271 (0.3 A g^{-1})	10 000	69
Curved graphene nanosheets	Hummer's method	256 (0.3 A g^{-1})	5000	38
Graphene oxide nanoribbons	Hummer's method	33 (1 A g^{-1})	Not mentioned	70
Curved graphene-MnO_2	Oxidation	236 (2 A g^{-1})	1000	63
$NiSe_2$/$CoSe_2$/CNT	Chemical precipitation	848 (2 A g^{-1})	1000	71
UzMWCNT/PPy	**Polymerisation**	**944 (1 A g^{-1})**	**5000**	**This work**

access to electrolytic ions. At high frequencies, materials with supercapacitance properties behave like resistors, while at low frequencies, they act as capacitors.

The impedance data were analyzed using Z-View software, employing the equivalent circuit model shown in Fig. 7c, which consists of a solution resistance (R_s) in series with a parallel combination of charge transfer resistance (R_{ct}) and capacitance (C).[72] The UzMWCNT/PPy composite exhibited a lower R_{ct} value compared to pristine UzMWCNT, indicating enhanced charge transfer kinetics and reduced interfacial resistance due to the incorporation of polypyrrole, which facilitates improved electronic conductivity and ion diffusion. Furthermore, the lower R_s value observed for UzMWCNT/PPy suggests improved electrolyte accessibility and enhanced electrode–electrolyte interaction.

Cycling performance is a critical factor when evaluating supercapacitor electrodes for practical applications. In this study, the electrochemical stability of the hybrid nanocomposite was assessed at a current density of 5 A g^{-1}, as depicted in Fig. 7b. The performance of supercapacitor devices is intricately linked to the cycling stability of the electrode material. The test conditions encompassed a voltage window spanning from −0.4 to 0.6 V, with a current density of 5 A g^{-1}. Remarkably, after 5000 cycles, the UzMWCNT/PPy electrode retained approximately 92% of its initial capacitance, indicating outstanding capacity reversibility throughout consecutive charge and discharge cycles.

It's worth noting that polypyrrole, when used as a standalone supercapacitor electrode, often exhibits poor cycling stability. However, the incorporation of UzMWCNT sheets in the composite serves as an effective means to restrain the swelling and shrinkage of polypyrrole during the polymerization process. This structural feature makes the hybrid material more adaptable to volumetric changes during redox reactions,

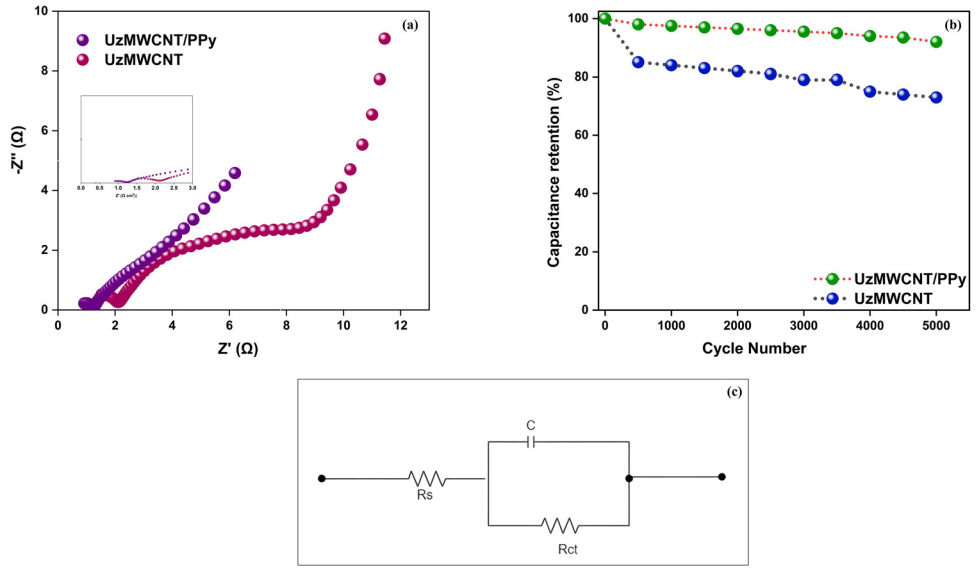

Fig. 7 (a) Nyquist plot of UzMWCNT and UzMWCNT/PPy nanocomposites; (b) cycling stability of the UzMWCNT and UzMWCNT/PPy nanocomposite electrode; and (c) Z-View software, employing the equivalent circuit model.

contributing to its enhanced cycling stability and overall performance as a supercapacitor electrode.

3.4. UzMWCNT/PPy asymmetric supercapacitor performance

To further assess the electrochemical performance of the UzMWCNT/PPy//AC composite, CV was conducted. Fig. 8a displays CV curves recorded at scan rates ranging from 5 to 100 mV s^{-1}, within a potential window of 0–1.6 V. The quasi-rectangular shape of these curves indicates the pseudocapacitive behavior of the UzMWCNT/PPy//AC composite. As the scan rate increases, the response current consistently rises, demonstrating that the ionic and electronic transport processes occur quickly enough to support

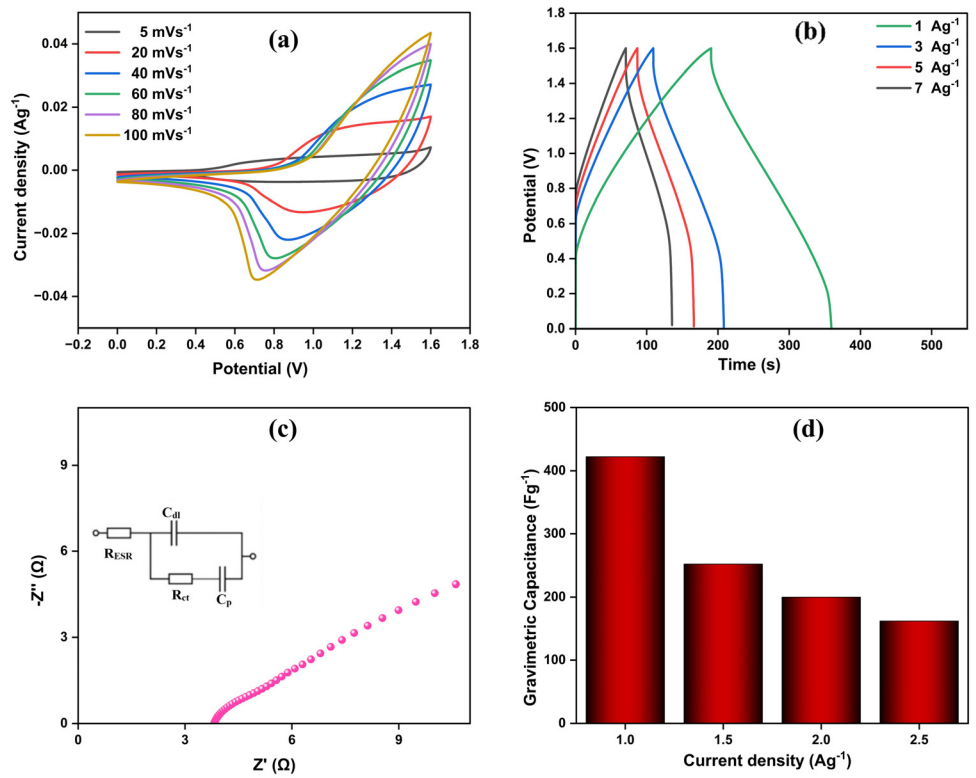

Fig. 8 Electrochemical performance evaluation of the UzMWCNT/PPy//AC asymmetric supercapacitor cell. (a) CV curves obtained at different scan rates; (b) GCD curves obtained at different current densities; (c) Nyquist plot of the fabricated cell; and (d) gravimetric capacitance at different current densities calculated for the cell.

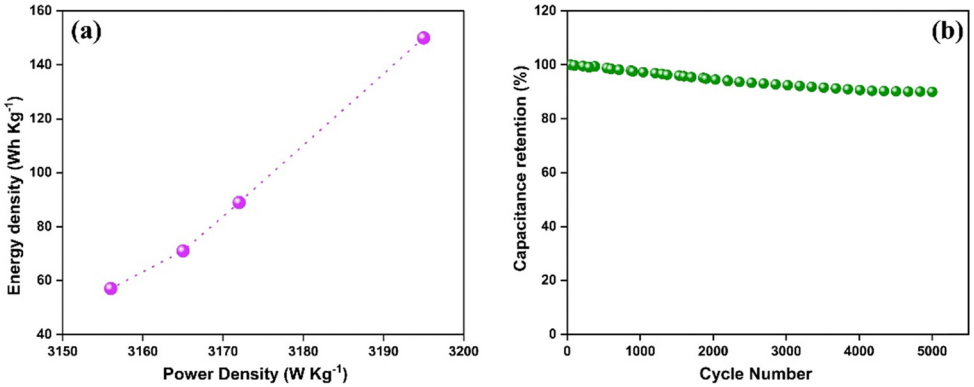

Fig. 9 (a) Ragone plot for the UzMWCNT/PPy//AC asymmetric supercapacitor cell and (b) cycling stability.

efficient charge transfer. Additionally, the consistent shape of the CV curves across different scan rates highlights the composite's excellent ionic and electronic conductivity.

Fig. 8b presents the GCD curves obtained at current densities of 1, 1.5, 2, and 2.5 A g^{-1}. The nearly linear curves suggest good symmetry and low internal resistance (minimal iR drop), characteristics indicative of a high-performing capacitor. As the current density increases, however, a gradual deviation from the linear and symmetrical shape becomes noticeable. This nonlinear behavior further confirms the pseudocapacitive nature of the composite, aligning with the redox peaks observed in the CV curves.

EIS measurements on the UzMWCNT/PPy//AC composite (Fig. 8c) show that in the high-frequency region, the semicircular arc indicates low internal resistance. In the low-frequency region, the steep slope suggests fast ion exchange during charge and discharge. The network structure of the UzMWCNT, combined with PPy, enhances the mobility of electrolyte ions during the exchange process. These findings demonstrate that the UzMWCNT/PPy//AC composite significantly improves the electrochemical performance of supercapacitors.

The bar graph shows the gravimetric capacitance of the UzMWCNT/PPy//AC composite at different current densities (1.0, 1.5, 2.0, and 2.5 A g^{-1}). At 1.0 A g^{-1}, the composite exhibits the highest gravimetric capacitance of approximately 400 F g^{-1}. As the current density increases, the gravimetric capacitance gradually decreases, with around 252 F g^{-1} at 1.5 A g^{-1}, 200 F g^{-1} at 2.0 A g^{-1}, and slightly below 162 F g^{-1} at 2.5 A g^{-1} (Fig. 8d). This reduction in capacitance at higher current densities is expected due to the limited ion diffusion and reduced utilization of the electrode's active surface. As the current density increases, ions in the electrolyte have less time to effectively reach the entire surface of the electrode, resulting in lower capacitance. Despite this, the UzMWCNT/PPy//AC composite maintains a substantial capacitance even at higher current densities, demonstrating its good rate capability.

The UzMWCNT/PPy//AC composite, when employed as an electrode material, exhibited excellent charge–discharge reversibility. This performance is attributed to the efficient storage and release of charge at the interface between the active electrode material and the electrolyte, demonstrating its potential for high-performance supercapacitor applications. The energy density (E) and power density (P) of the device were further evaluated using the corresponding equations.[73–75]

$$E = \frac{c_{sp}(\Delta v)^2}{2} \quad (2)$$

$$P = \frac{E}{\Delta t} \quad (3)$$

Energy density is given in W h kg^{-1} and is determined using the specific capacitance (C_{sp}) and the potential shift (ΔV) squared. Power density is represented in W kg^{-1} and is calculated using the energy (E) and time (Δt in s).

Using the calculated formula, the specific capacitance, energy density, and power density of the UzMWCNT/PPy//AC composite at varying current densities are shown in Fig. 9a. The fabricated asymmetric supercapacitor cell demonstrates excellent capacitive behavior, achieving an energy density of 150 W h kg^{-1} with a corresponding power density of 3195 W kg^{-1}. Table 2 summarizes recent studies on supercapacitor electrodes utilizing

Table 2 Performance comparison of PPy/CNT supercapacitor electrodes

Supercapacitor electrodes	Method	Power density (W kg^{-1})	Energy density (W h kg^{-1})	Ref.
Polypyrrole/carbon nanotube	Electrodeposition	402	31.2	76
Polypyrrole/carbon nanotube	Chemical vapor deposition	1051	3.57	77
Copper-doped PPy/MWCNT	Oxidative polymerization	19.89	4479	78
Polypyrrole/graphene oxide/multi-walled carbon nanotubes	Electropolymerization	441.24	40.45	79
CO3o4@Polypyrrole/Mwcnt	Hydrothermal process	1500	84.58	80
UzMWCNT/PPy	**Modified Hummer's process**	**3195**	**150**	**This work**

PPy and CNT composites, highlighting their fabrication methods and corresponding energy and power densities.

The cycling stability of the fabricated cell was evaluated over 5000 charge–discharge cycles at a current density of 5 A g^{-1} (Fig. 9b). The cell exhibited exceptional performance, maintaining 95% of its initial capacitance, which highlights its durability and the stability of the electrochemical system.

4. Conclusion

The unzipped MWCNT/polypyrrole (UzMWCNT/PPy) composite electrodes demonstrated exceptional electrochemical performance, making them a promising candidate for high-performance supercapacitor applications. The novel unzipping method, achieved through a modified Hummer's process followed by reduction, effectively transformed multi-walled carbon nanotubes into UzMWCNT with enhanced structural and functional properties. The hybrid UzMWCNT/PPy composite exhibited a high specific capacitance of 944 F g^{-1} at 1 A g^{-1}, excellent cycling stability with 92% capacitance retention after 5000 cycles, and impressive gravimetric capacitance retention of approximately 95% in an asymmetric configuration with active carbon electrodes. The synergistic integration of UzMWCNT and PPy enabled superior pseudocapacitive behavior, improved ion transport, and enhanced charge storage capabilities. The increased surface area, mesoporous structure, and tailored conductivity of the composite contributed to its remarkable energy storage performance. These findings highlight the potential of UzMWCNT/PPy composites in developing next-generation energy storage devices with high energy density, excellent cycling stability, and robust durability.

Data availability

The data that support the findings of this study are available from the corresponding author upon reasonable request.

Conflicts of interest

There are no conflicts to declare.

Acknowledgements

We acknowledge the Centre for Research, CHRIST University, for the support provided for this research work.

References

1 S. Lebaschi, M. Hekmati and H. Veisi, Green synthesis of palladium nanoparticles mediated by black tea leaves (Camellia sinensis) extract: Catalytic activity in the reduction of 4-nitrophenol and Suzuki-Miyaura coupling reaction under ligand-free conditions, *J. Colloid Interface Sci.*, 2017, **485**, 223–231, DOI: **10.1016/j.jcis.2016.09.027**.

2 K. Han, Y. Liu, H. Huang, Q. Gong, Z. Zhang and G. Zhou, Tremella-like NiO microspheres embedded with fish-scale-like polypyrrole for high-performance asymmetric supercapacitor, *RSC Adv.*, 2019, **9**(38), 21608–21615, DOI: **10.1039/c9ra03046h**.

3 S. Simon, N. James and P. B. Sreeja, Water hyacinth-poly(3,4-Ethylenedioxythiophene) composite as a facile electrode for supercapacitor application, *Mater Today Proc.*, 2023, DOI: **10.1016/j.matpr.2023.10.068**.

4 D. N. Bangera, Y. N. Sudhakar and R. A. Nazareth, Concrete-based energy storage: exploring electrode and electrolyte enhancements, *RSC Adv.*, 2024, **14**(39), 28854–28880, DOI: **10.1039/d4ra04812a**.

5 I. Beyers, A. Bensmann and R. Hanke-Rauschenbach, Ragone plots revisited: A review of methodology and application across energy storage technologies, *J Energy Storage*, 2023, **73**, 109097, DOI: **10.1016/j.est.2023.109097**PD.

6 Y. Liu, S. P. Jiang and Z. Shao, Intercalation pseudocapacitance in electrochemical energy storage: recent advances in fundamental understanding and materials development, *Mater Today Adv.*, 2020, **7**, 100072, DOI: **10.1016/j.mtadv.2020.100072**.

7 M. Zhong, M. Zhang and X. Li, Carbon nanomaterials and their composites for supercapacitors, *Carbon Energy*, 2022, **4**(5), 950–985, DOI: **10.1002/cey2.219**.

8 D. Nandi, V. B. Mohan, A. K. Bhowmick and D. Bhattacharyya, Metal/metal oxide decorated graphene synthesis and application as supercapacitor: a review, *J. Mater. Sci.*, 2020, **55**(15), 6375–6400, DOI: **10.1007/s10853-020-04475-z**.

9 R. Kumar, E. Joanni and S. Sahoo, *et al.*, An overview of recent progress in nanostructured carbon-based supercapacitor electrodes: From zero to bi-dimensional materials, *Carbon*, 2022, **193**, 298–338, DOI: **10.1016/j.carbon.2022.03.023**.

10 L. Wang, G. Yang, S. Peng, J. Wang, W. Yan and S. Ramakrishna, One-dimensional nanomaterials toward electrochemical sodium-ion storage applications via electrospinning, *Energy Storage Mater.*, 2020, **25**, 443–476, DOI: **10.1016/J.ENSM.2019.09.036**.

11 O. S. Adedoja, E. R. Sadiku and Y. Hamam, An Overview of the Emerging Technologies and Composite Materials for Supercapacitors in Energy Storage Applications, *Polymers*, 2023, **15**(10), 1–32, DOI: **10.3390/polym15102272**.

12 S. Kamila, B. K. Jena and S. Basu, Advances in Electrochemical Energy Storage Device: Supercapacitor, *Energy Storage*, 2021, pp. 119–147, DOI: **10.1002/9781119555599.ch4**.

13 E. Mossali, N. Picone, L. Gentilini, O. Rodrìguez, J. M. Pérez and M. Colledani, Lithium-ion batteries towards circular economy: A literature review of opportunities and issues of recycling treatments, *J. Environ. Manage.*, 2020, 264, DOI: **10.1016/j.jenvman.2020.110500**.

14 R. Hemmati and H. Saboori, Emergence of hybrid energy storage systems in renewable energy and transport applications – A review, *Renewable Sustainable Energy Rev.*, 2016, **65**, 11–23, DOI: **10.1016/j.rser.2016.06.029**.

15 R. Mondal, N. K. Mishra, T. Maiyalagan, A. Gupta and P. Singh, $La_{1-x}K_xFeO_{3-\delta}$: An Anion Intercalative Pseudocapacitive Electrode for Supercapacitor Application, *ACS Omega*, 2021, **6**(45), 30488–30498, DOI: **10.1021/acsomega.1c03902**.

16 C. Ma, J. Bai, M. Demir, X. Hu, S. Liu and L. Wang, Water chestnut shell-derived N/S-doped porous carbons and their

applications in CO_2 adsorption and supercapacitor, *Fuel*, 2022, **326**, 125119, DOI: 10.1016/J.FUEL.2022.125119.

17 R. Farma, Y. Tania and I. Apriyani, Conversion of hazelnut seed shell biomass into porous activated carbon with KOH and CO_2 activation for supercapacitors, *Mater Today Proc.*, 2023, **87**, 51–56, DOI: 10.1016/J.MATPR.2023.02.099.

18 D. R. Lobato-Peralta, P. U. Okoye and C. Alegre, A review on carbon materials for electrochemical energy storage applications: State of the art, implementation, and synergy with metallic compounds for supercapacitor and battery electrodes, *J. Power Sources*, 2024, **617**(July), DOI: 10.1016/j.jpowsour.2024.235140.

19 D. K. Singha, R. I. Mohanty, P. Bhanja and B. K. Jena, Metal-organic framework and graphene composites: advanced materials for electrochemical supercapacitor applications, *Mater. Adv.*, 2023, **4**(20), 4679–4706, DOI: 10.1039/d3ma00523b.

20 M. Huang, L. Wang and S. Chen, *et al.*, Highly flexible all-solid-state cable-type supercapacitors based on Cu/reduced graphene oxide/manganese dioxide fibers, *RSC Adv.*, 2017, **7**(17), 10092–10099, DOI: 10.1039/c6ra28117f.

21 T. E. Balaji, H. Tanaya Das and T. Maiyalagan, Recent Trends in Bimetallic Oxides and Their Composites as Electrode Materials for Supercapacitor Applications, *ChemElectroChem*, 2021, **8**(10), 1723–1746, DOI: 10.1002/celc.202100098.

22 G. B. Pour, H. Ashourifar, L. F. Aval and S. Solaymani, CNTs-Supercapacitors: A Review of Electrode Nanocomposites Based on CNTs, Graphene, Metals, and Polymers, *Symmetry*, 2023, **15**(6), 1–16, DOI: 10.3390/sym15061179.

23 M. Jasna, M. Muraleedharan Pillai, A. Abhilash, P. S. Midhun, S. Jayalekshmi and M. K. Jayaraj, Polyaniline wrapped carbon nanotube/exfoliated MoS2 nanosheet composite as a promising electrode for high power supercapacitors, *Carbon Trends*, 2022, **7**, 100154, DOI: 10.1016/J.CARTRE.2022.100154.

24 B. O. Murjani, P. S. Kadu, M. Bansod, S. S. Vaidya and M. D. Yadav, Carbon nanotubes in biomedical applications: current status, promises, and challenges, *Carbon Lett.*, 2022, **32**(5), 1207–1226, DOI: 10.1007/s42823-022-00364-4.

25 S. B. Abitkar, P. R. Jadhav, N. L. Tarwal, A. V. Moholkar and C. E. Patil, A facile synthesis of α-$Ni(OH)_2$-CNT composite films for supercapacitor application, *Adv. Powder Technol.*, 2019, **30**(10), 2285–2292, DOI: 10.1016/j.apt.2019.07.008.

26 J. Ouyang, Applications of carbon nanotubes and graphene for third-generation solar cells and fuel cells, *Nano Mater Sci.*, 2019, **1**(2), 77–90, DOI: 10.1016/j.nanoms.2019.03.004.

27 G. A. Snook, P. Kao and A. S. Best, Conducting-polymer-based supercapacitor devices and electrodes, *J. Power Sources*, 2011, **196**(1), 1–12, DOI: 10.1016/J.JPOWSOUR.2010.06.084.

28 S. Zhu, J. Ni and Y. Li, Carbon nanotube-based electrodes for flexible supercapacitors, *Nano Res.*, 2020, **13**(7), 1825–1841, DOI: 10.1007/s12274-020-2729-5.

29 P. Lv, Y. Meng, L. Song, H. Pang and W. Liu, A self-supported electrode for supercapacitors based on nanocellulose/multi-walled carbon nanotubes/polypyrrole composite, *RSC Adv.*, 2020, **11**(2), 1109–1114, DOI: 10.1039/d0ra08040c.

30 C. L. Lin, J. W. Li, Y. F. Chen, J. X. Chen, C. C. Cheng and C. W. Chiu, Graphene Nanoplatelet/Multiwalled Carbon Nanotube/Polypyrrole Hybrid Fillers in Polyurethane Nanohybrids with 3D Conductive Networks for EMI Shielding, *ACS Omega*, 2022, **7**(49), 45697–45707, DOI: 10.1021/acsomega.2c06613.

31 R. Khare, D. B. Shinde and S. Bansode, *et al.*, Graphene nanoribbons as prospective field emitter, *Appl. Phys. Lett.*, 2015, **106**(2), DOI: 10.1063/1.4905473.

32 J. Parayangattil Jyothibasu, M. Z. Chen and R. H. Lee, Polypyrrole/Carbon Nanotube Freestanding Electrode with Excellent Electrochemical Properties for High-Performance All-Solid-State Supercapacitors, *ACS Omega*, 2020, **5**(12), 6441–6451, DOI: 10.1021/acsomega.9b04029.

33 M. M. Rahman Khan and M. M. H. Rumon, Recent Progress on the Synthesis, Morphological Topography, and Battery Applications of Polypyrrole-Based Nanocomposites, *Polymers*, 2024, (23), 16, DOI: 10.3390/polym16233277.

34 P. Mahajan, S. Sardana and A. Mahajan, 1D graphene nanoribbons-mediated defect engineering in 2D MXene for high-performance supercapacitors, *Appl. Phys. Lett.*, 2024, **124**(11), DOI: 10.1063/5.0179060.

35 H. Pan, J. Li and Y. P. Feng, Carbon nanotubes for supercapacitor, *Nanoscale Res. Lett.*, 2010, **5**(3), 654–668, DOI: 10.1007/s11671-009-9508-2.

36 A. Aphale, K. Maisuria, M. K. Mahapatra, A. Santiago, P. Singh and P. Patra, Hybrid Electrodes by In-Situ Integration of Graphene and Carbon-Nanotubes in Polypyrrole for Supercapacitors OPEN, *Sci. Rep.*, 2015, **5**, 14445, DOI: 10.1038/srep14445.

37 A. K. Geim and K. S. Novoselov, *The Rise of Graphene*. https://www.nature.com/naturematerials.

38 H. Wang, Y. Wang, Z. Hu and X. Wang, Cutting and unzipping multiwalled carbon nanotubes into curved graphene nanosheets and their enhanced supercapacitor performance, *ACS Appl. Mater. Interfaces*, 2012, **4**(12), 6827–6834, DOI: 10.1021/am302000z.

39 S. Abdalla, F. Al-Marzouki, A. A. Al-Ghamdi and A. Abdel-Daiem, Different Technical Applications of Carbon Nanotubes, *Nanoscale Res. Lett.*, 2015, **10**(1), DOI: 10.1186/s11671-015-1056-3.

40 B. Zhang, F. Kang, J. M. Tarascon and J. K. Kim, Recent advances in electrospun carbon nanofibers and their application in electrochemical energy storage, *Prog. Mater. Sci.*, 2016, **76**, 319–380, DOI: 10.1016/j.pmatsci.2015.08.002.

41 M. F. L. De Volder, S. H. Tawfick, R. H. Baughman and A. John Hart, Carbon Nanotubes: Present and Future Commercial Applications, *Science*, 2013, **339**(6119), 535–539.

42 T. Otowa, R. Tanibata and M. Itoh, Production and adsorption characteristics of MAXSORB: High-surface-area active carbon, *Gas Sep. Purif.*, 1993, **7**(4), 241–245, DOI: 10.1016/0950-4214(93)80024-Q.

43 L. J. Moriau, M. Bele and A. Vižintin, *et al.*, Synthesis and Advanced Electrochemical Characterization of Multifunctional Electrocatalytic Composite for Unitized Regenerative Fuel Cell, *ACS Catal.*, 2019, **9**(12), 11468–11483, DOI: 10.1021/acscatal.9b03385.

44 R. A. Fisher, M. R. Watt and W. Jud Ready, Functionalized Carbon Nanotube Supercapacitor Electrodes: A Review on Pseudocapacitive Materials, *ECS J. Solid State Sci. Technol.*, 2013, **2**(10), M3170–M3177, DOI: **10.1149/2.017310jss**.

45 L. Shahriary and A. A. Athawale, Graphene Oxide Synthesized by using Modified Hummers Approach, *Int. J. Renewable Energy Environ. Eng.*, 2014, **02**(01), 58–63.

46 R. K. L. Tan, S. P. Reeves and N. Hashemi, *et al.*, Graphene as a flexible electrode: Review of fabrication approaches, *J. Mater. Chem. A*, 2017, **5**(34), 17777–17803, DOI: **10.1039/c7ta05759h**.

47 Y. Shi, L. Pan and B. Liu, *et al.*, Nanostructured conductive polypyrrole hydrogels as high-performance, flexible supercapacitor electrodes, *J. Mater. Chem. A*, 2014, **2**(17), 6086–6091, DOI: **10.1039/c4ta00484a**.

48 S. Reich, M. Burgard and M. Langner, *et al.*, Polymer nanofibre composite nonwovens with metal-like electrical conductivity, *npj Flexible Electron.*, 2018, **2**(1), 5, DOI: **10.1038/s41528-017-0018-5**.

49 J. Xue, Q. Sun, Y. Zhang, W. Mao, F. Li and C. Yin, Preparation of a Polypyrrole/Graphene Oxide Composite Electrode by Electrochemical Codeposition for Capacitor Deionization, *ACS Omega*, 2020, **5**, 10995–11004, DOI: **10.1021/acsomega.0c00817**.

50 Q. Meng, K. Cai, Y. Chen and L. Chen, Research progress on conducting polymer based supercapacitor electrode materials, *Nano Energy*, 2017, **36**, 268–285, DOI: **10.1016/j.nanoen.2017.04.040**.

51 K. R. Thines, E. C. Abdullah, N. M. Mubarak and M. Ruthiraan, In-situ polymerization of magnetic biochar – polypyrrole composite: A novel application in supercapacitor, *Biomass Bioenergy*, 2017, **98**, 95–111, DOI: **10.1016/j.biombioe.2017.01.019**.

52 A. Moyseowicz, K. Pajak, K. Gajewska and G. Gryglewicz, Synthesis of polypyrrole/reduced graphene oxide hybrids via hydrothermal treatment for energy storage applications, *Materials*, 2020, (10), 13, DOI: **10.3390/ma13102273**.

53 J. P. Jyothibasu, M. Z. Chen and Y. C. Tien, *et al.*, V2o5/carbon nanotube/polypyrrole based freestanding negative electrodes for high-performance supercapacitors, *Catalysts*, 2021, **11**(8), 1–15, DOI: **10.3390/catal11080980**.

54 Y. Cong, S. Liu and H. Chen, Fabrication of Conductive Polypyrrole Nanofibers by Electrospinning, *J. Nanomater.*, 2013, 2013, DOI: **10.1155/2013/148347**.

55 A. Yussuf, M. Al-Saleh, S. Al-Enezi and G. Abraham, Synthesis and Characterization of Conductive Polypyrrole: The Influence of the Oxidants and Monomer on the Electrical, Thermal, and Morphological Properties, *Int. J. Polym. Sci.*, 2018, 2018, DOI: **10.1155/2018/4191747**.

56 A. Cortijo and M. A. H. Vozmediano, Electronic properties of curved graphene sheets, *EPL*, 2007, **77**(4), 1–4, DOI: **10.1209/0295-5075/77/47002**.

57 S. S. Siwal, Q. Zhang, N. Devi and V. K. Thakur, Carbon-based polymer nanocomposite for high-performance energy storage applications, *Polymers*, 2020, **12**(3), 1–30, DOI: **10.3390/polym12030505**.

58 J. Jang and H. Yoon, Facile fabrication of polypyrrole nanotubes using reverse microemulsion polymerization, *Chem. Commun.*, 2003, 720–721, DOI: **10.1039/b211716a**.

59 A. Laforgue, All-textile flexible supercapacitors using electrospun poly(3,4-ethylenedioxythiophene) nanofibers, *J. Power Sources*, 2011, **196**(1), 559–564, DOI: **10.1016/J.JPOWSOUR.2010.07.007**.

60 J. Zhang and X. S. Zhao, Conducting polymers directly coated on reduced graphene oxide sheets as high-performance supercapacitor electrodes, *J. Phys. Chem. C*, 2012, **116**(9), 5420–5426, DOI: **10.1021/jp211474e**.

61 K. H. An, K. K. Jeon, J. K. Heo, S. C. Lim, D. J. Bae and Y. H. Lee, High-Capacitance Supercapacitor Using a Nanocomposite Electrode of Single-Walled Carbon Nanotube and Polypyrrole, *J. Electrochem. Soc.*, 2002, **149**(8), A1058, DOI: **10.1149/1.1491235**.

62 Q. Cheng, J. Tang, J. Ma, H. Zhang, N. Shinya and L. C. Qin, Graphene and carbon nanotube composite electrodes for supercapacitors with ultra-high energy density, *Phys. Chem. Chem. Phys.*, 2011, **13**(39), 17615–17624, DOI: **10.1039/c1cp21910c**.

63 X. Y. Li, Q. Wang and H. W. Wang, Conversion of carbon nanotubes into curved graphene with improved capacitance, *New Carbon Mater.*, 2021, **36**(4), 835–842, DOI: **10.1016/S1872-5805(21)60086-0**.

64 Y. Zhu, K. Shi and I. Q. Zhitomirsky, *J. Power Sources*, 2014, **268**(January 2018), 233–239, DOI: **10.1016/j.jpowsour.2014.06.046**.

65 C. Li, X. Zhang and G. Qu, *et al.*, Highly Reversible Zn Metal Anode Securing by Functional Electrolyte Modulation, *Adv Energy Mater.*, 2024, **2400872**, 1–10, DOI: **10.1002/aenm.202400872**.

66 J. Zhu, X. F. Lu, D. Luan and X. W. Lou, Metal–Organic Frameworks Derived Carbon-Supported Metal Electrocatalysts for Energy-Related Reduction Reactions, *Angew. Chem., Int. Ed.*, 2024, 202408846, DOI: **10.1002/anie.202408846**.

67 R. Hajare, S. Kempahanumakkagaari, T. Ramakrishnappa, A. Saniya, K. Sourav and A. Amrutha, Study of advances in carbon composites as electrodes for supercapacitors, *Mater Today Proc.*, 2022, **49**, 650–659, DOI: **10.1016/j.matpr.2021.05.164**.

68 S. S. Shah, E. Cevik, M. A. Aziz, T. F. Qahtan, A. Bozkurt and Z. H. Yamani, Jute Sticks Derived and Commercially Available Activated Carbons for Symmetric Supercapacitors with Bio-electrolyte: A Comparative Study, *Synth. Met.*, 2021, **277**(January), DOI: **10.1016/j.synthmet.2021.116765**.

69 Q. Cheng, J. Tang, N. Shinya and L. C. Qin, Polyaniline modified graphene and carbon nanotube composite electrode for asymmetric supercapacitors of high energy density, *J. Power Sources*, 2013, **241**, 423–428, DOI: **10.1016/j.jpowsour.2013.04.105**.

70 M. Fathi, M. Saghafi and F. Mahboubi, Graphene oxide nanoribbons and their applications in supercapacitors, *J. Ultrafine Grained Nanostruct. Mater.*, 2014, **47**(2), 71–76.

71 J. Zheng and X. Bai, Preparation of Ni-Co PBA-derived beaded $NiSe_2/CoSe_2$/CNT for high-performance supercapacitors,

J. Alloys Compd., 2023, **944**, 169110, DOI: **10.1016/j.jallcom.2023.169110**.

72 N. Li, X. Zhang and S. Zhao, *et al.*, Amorphous nickel borate nanosheets as cathode material with high capacity and better cycling performance for zinc ion battery, *Chin. Chem Lett.*, 2023, **34**(6), 38–41, DOI: **10.1016/j.cclet.2022.07.012**.

73 U. Thubsuang, S. Laebang, N. Manmuanpom, S. Wongkasemjit and T. Chaisuwan, Tuning pore characteristics of porous carbon monoliths prepared from rubber wood waste treated with H3PO4 or NaOH and their potential as supercapacitor electrode materials, *J. Mater. Sci.*, 2017, **52**(11), 6837–6855, DOI: **10.1007/s10853-017-0922-z**.

74 A. B. Ganganboina, A. D. Chowdhury and R. Doong, Nano assembly of N-doped graphene quantum dots anchored Fe_3O_4/halloysite nanotubes for high performance supercapacitor, *Electrochim. Acta*, 2017, **245**, 912–923, DOI: **10.1016/j.electacta.2017.06.002**.

75 A. Jeyaranjan, T. S. Sakthivel, C. J. Neal and S. Seal, Scalable ternary hierarchical microspheres composed of PANI/rGO/CeO2 for high performance supercapacitor applications, *Carbon*, 2019, **151**, 192–202, DOI: **10.1016/j.carbon.2019.05.043**.

76 R. Xu, J. Wei and F. Guo, *et al.*, Highly conductive, twistable and bendable polypyrrole-carbon nanotube fiber for efficient supercapacitor electrodes, *RSC Adv.*, 2015, **5**(28), 22015–22021, DOI: **10.1039/c5ra01917f**.

77 H. Lee, H. Kim, M. S. Cho, J. Choi and Y. Lee, Fabrication of polypyrrole (PPy)/carbon nanotube (CNT) composite electrode on ceramic fabric for supercapacitor applications, *Electrochim. Acta*, 2011, **56**(22), 7460–7466, DOI: **10.1016/j.electacta.2011.06.113**.

78 K. Mounika, B. Anupama, J. Pragathi and C. Gyanakumari, *J. Sci. Res.*, 2010, **2**, 513–524, DOI: **10.3329/jsr.v2i3.4899**.

79 M. A. A. Mohd Abdah, N. S. Mohd Razali, P. T. Lim, S. Kulandaivalu and Y. Sulaiman, One-step potentiostatic electrodeposition of polypyrrole/graphene oxide/multi-walled carbon nanotubes ternary nanocomposite for supercapacitor, *Mater. Chem. Phys.*, 2018, **219**(June), 120–128, DOI: **10.1016/j.matchemphys.2018.08.018**.

80 S. Ramesh, Y. Haldorai, H. S. Kim and J. H. Kim, A nanocrystalline Co_3O_4@polypyrrole/MWCNT hybrid nanocomposite for high performance electrochemical supercapacitors, *RSC Adv.*, 2017, **7**(58), 36833–36843, DOI: **10.1039/c7ra06093a**.